Nature of Paramagnetic Species in Nitrogen-Doped SnO2: A Combined Electron Paramagnetic Resonance and Density Functional Theory Study

Albanese, Elisa; Di Valentin, Cristiana; Pacchioni, Gianfranco; Sauvage, Frédéric; Livraghi, Stefano; Giamello, Elio. Nature of Paramagnetic Species in Nitrogen-Doped SnO2: A Combined Electron Paramagnetic Resonance and Density Functional Theory Study. JOURNAL OF PHYSICAL CHEMISTRY. C, NANOMATERIALS AND INTERFACES. 119 (48) pp: 26895-26903.
DOI: 10.1021/acs.jpcc.5b09613

Nature of Paramagnetic Species in Nitrogen-doped SnO_2: A Combined Electron Paramagnetic Resonance and Density Functional Theory Study

Elisa Albanese,[†] Cristiana Di Valentin,[*,†] Gianfranco Pacchioni,[†] Frédéric Sauvage,[§] Stefano Livraghi[‡] and Elio Giamello[‡]

[†]Dipartimento di Scienza dei Materiali, Università Milano Bicocca, via R. Cozzi, 55 – 20125 Milano, Italy

[§]Laboratoire de Réactivité et Chimie des Solides (CNRS UMR 7314), Université de Picardie Jules Verne, 33 rue Saint-Leu, 80039 Amiens Cedex, France

[‡]Dipartimento di Chimica and NIS, Università di Torino, Via P. Giuria 7, I - 10125 Torino, Italy

ABSTRACT: A combination of electron paramagnetic resonance (EPR) spectra and density functional theory (DFT) calculations is used to characterize the paramagnetic species in rutile N-doped SnO_2 samples synthesized by wet chemistry methods. In particular, the nature of paramagnetic N species, substitutional or interstitial, and their effect on the electronic structure are discussed. Complex EPR spectra generated by the interaction of the unpaired electron with N and Sn nuclei have been accurately simulated to obtain the EPR properties (**g** and **A** tensors). The results suggest that the N dopants form a rather symmetric structure with three magnetically equivalent or nearly equivalent Sn atoms surrounding the N impurity. After a careful assessment of an all electron basis set for Sn atoms, realistic models of substitutional and interstitial N-doped SnO_2 structures have been designed, and the corresponding hyperfine coupling constants (hpcc) computed. The comparison between computed and measured hpcc values leads to the assignment of the paramagnetic centres in N-SnO_2 to substitutional N dopants that take the position of the O atoms in the lattice. The DFT calculations finally suggest the N impurities induce the formation of localized empty states (electron holes) in the intra bandgap.

INTRODUCTION

SnO_2 is a multifunctional oxide semiconductor finding application in several fields, such as chemical sensors,[1] lithium-ion batteries,[2] solar cells,[3] catalysis,[4] etc. With a bandgap of 3.6 eV, SnO_2 is also a promising material for ultraviolet light emitting diodes (LED) and photodetectors.[5] It has also been proposed as building block for junctions in opto-electronic devices.[6] However, in this case, it is essential to obtain a p-type doping of the material. Undoped SnO_2 is characterized by an intrinsic n-type conduction due to native oxygen vacancy defects. The p-type doping has been tried via cation doping, but nitrogen is also an excellent possibility due to the high solubility and non-toxicity. Nitrogen doped SnO_2 (N-SnO_2 in the following) has also been considered for the preparation of diluted magnetic semiconductors of potential used for spintronics,[7, 8] although this prospect stems mostly from Density Functional Theory (DFT) calculations being a highly controversial topic. Owing to the large bandgap of 3.6 eV, SnO_2 cannot exploit visible light for photocatalysis. As for many other semiconducting oxides, various strategies have been explored to extend the photocatalytic activity towards the visible range, such as doping, nanostructuring, surface modification or functionalization, formation of hetero-composite materials.[9,10,11] In many cases, SnO_2 has been mixed with other photocatalysts (TiO_2, ZnO, etc.) to form composite photo-electrodes. By contrast to the case of the anatase TiO_2, for which the doping of its crystal structure has been extensively studied by taking advantage of its sensitiveness to the introduction of punctual defects resulting from its $3d^0$ electronic configuration[12,13], there are only very few reports dealing with doping for shifting SnO_2's absorption tails towards visible light.[14,15,16]

The inclusion of nitrogen dopant into the SnO_2 lattice is a credible approach to tune the absorption properties, either via bandgap narrowing or by introducing new energy states into the gap. N-SnO_2 films have been prepared by magnetron reactive sputtering in gas mixtures of nitrogen and oxygen.[17] It was found that the optical band gap decreases when increasing nitrogen partial pressure into the sputtering chamber. Earlier work on N-doped SnO_2 showed only limited band gap shift, probably because substitutional nitrogen doping was not achieved.[16,18] On the contrary, a large band gap narrowing has been reported on atomic N-doping of SnO_2 submicrorod arrays by reactive magnetron sputtering. In this case, a large red-shift up to 1.9 eV was reported together with very appealing photocatalytic properties driven by incident visible light irradiation.[19]

N-SnO_2 has been previously studied by first principle calculations.[7, 8, 20] However, all the results reported so far are based on standard GGA functionals, which are known to give an inaccurate description of the oxide electronic structure, in particular for the energy band gap description and localization of magnetic states.[21] In this work, we employed a hybrid DFT functional (B3LYP) particularly appropriated to describe very properly the band gap and the spin properties of solid systems.[22, 31] We report on very detailed theoretical calculation supported by careful experimental investigations to reveal the nature of nitrogen dopants in SnO_2. For this, a series of N-SnO_2 samples have been synthesized by precipitation followed by thermal post-annealing and the nature of the paramagnetic impurities analyzed by means of Electron Paramagnetic Resonance (EPR) spectra. The interaction of the unpaired electron with the ^{14}N and $^{117}Sn/^{119}Sn$ isotopes leads to complex EPR spectra that have been accurately simulated in order to derive robust EPR parameters (**g** and **A** tensors). The calculation from first principles of the physical properties of N-impurities in substitutional or interstitial positions in the SnO_2 lattice leads to a set of computed EPR properties compared to the measured ones. From the combination of measured and computed properties of the paramagnetic defects, we are proposing a robust assignment of the observed features to N atoms substituting O in the SnO_2 lattice, as tentatively suggested in the literature.[23]

The manuscript is organized as follow. In Section 2 we provide details on the experimental and computational methods used. Section 3.1 reports the experimental data and is divided in subsections dedicated to the signal arising from the N atoms of the defect centers (§ 3.1), to the symmetry of the defective site and isotopomers distribution (§ 3.1.1) and to the spin density of the N center in SnO_2 (§ 3.1.2). The results of DFT calculations are reported in Section 3.2 and are grouped in three subsections, regarding the calibration of Sn all electron basis set (§3.2.1), the structural model and electronic properties (§ 3.2.2), and, finally, the hyperfine constants (§ 3.2.3). A general discussion and the conclusions are reported in Section 4.

EXPERIMENTAL AND THEORETICAL METHODS

Preparation of N-SnO. Nitrogen doped SnO_2 materials (here after N-SnO_2) were prepared by precipitation. For this, typical synthesis involved $SnCl_4 \cdot 5H_2O$ (2.3g) and NH_4Cl (0.67g) dissolved in 50 ml of water. Then NaOH 1M was added into the solution dropwise until obtaining an exact pH of 8.0 to trigger the precipitation of the hydroxide. The precipitate obtained in this way was collected by centrifugation and washed with distilled water several times. The products were dried at 333 K overnight and finally calcined at 773 K for 1h. XRD analysis confirmed that the material is characterized by the rutile type structure (cassiterite) typical of SnO_2.

Two distinct ^{15}N containing N-SnO_2 samples were also prepared using 70% and 98% ^{15}N enriched NH_4Cl sample following the same procedure above described.

X-band Continuous Wave (CW) EPR spectra have been recorded on a Bruker EMX spectrometer equipped with a cylindrical cavity and operating at a 100 kHz field modulation. The measurements were carried out at room temperature (RT) and liquid nitrogen temperature (77 K) in cells that can be connected to a conventional high-vacuum apparatus (residual pressure < 10^{-4} mbar).

Q-band Continuous Wave (CW) EPR spectra have been recorded on a Bruker ELEXYS 580 operating at a 50 kHz field modulation. The Q-band spectra were recorded at room temperature (RT). Computer simulation of the spectra were obtained using the SIM32 program.

Periodic DFT calculations. The investigation of the N-doped SnO_2 was carried out with periodic DFT calculations employing the Becke-3[24] and Lee-Yang-Parr[25] (B3LYP) exchange and correlation functional as implemented in the CRYSTAL[26] program. Hybrid functionals are well-known to provide an accurate description of spin-polarized systems.[27,32]

Crystalline orbitals are represented as linear combinations of Bloch functions (BF) and are evaluated over a regular three-dimensions mesh of points in reciprocal space. Each BF is built from local atomic orbitals (AO) resulting from contractions (i.e. linear combinations with constant coefficients) of Gaussian-type-functions which in turn are the product of a Gaussian times a real solid spherical harmonic function. All electron basis set have been used for O and N atoms: 8-411G* and 7-311G*, respectively. For Sn we used different basis set (BS): an effective core potential (ECP), referred to as Barthelat and Durand-21G*,[28,29] and several all electron basis sets, as described below. With the most accurate all electron basis set on Sn (QZP) the computed Kohn-Sham band gap is 3.51 eV, in excellent agreement with the experimental band gap of 3.6 eV.

For the numerical integration of exchange-correlation term, 75 radial points and 974 angular points (XLGRID) in a Lebedev scheme in the region of chemical interest were adopted. The Pack-Monkhorst/Gilat shrinking factors for the reciprocal space were set to 6 for the SnO_2 pure system and to 4 for N-SnO_2, corresponding respectively to 40 and 36 real reciprocal space points at which the Hamiltonian matrix was diagonalized.

The calculations of the N-SnO_2 structures were performed on a 72 atoms pseudo-cubic supercell, corresponding to a 2x2x3 unit cell of rutile SnO_2. The optimized cell of the non-defective system is consistent with the experimental values (see Supporting Information). The accuracy of the integral calculations was increased with respect to its default value by setting the tolerances to 7, 7, 7, 7 and 18. The self-consistent field (SCF) iterative procedure converged to a tolerance in total energy of $\Delta E = 1 \cdot 10^{-7}$ a.u. The above computational parameters ensured a full numerical convergence on all the computed properties described in this work. All the crystal structures are fully optimized (i.e. both cell parameters and internal coordinates) without symmetry operators in order to allow a complete structural relaxation. However, the cell parameters of the SnO_2 are not much affected by the N inclusion. The percentage differences of the doped cells with respect the undoped one is, indeed, always below 1%.

The hyperfine spin-Hamiltonian, $H_{hfc} = S \bullet A \bullet I$, is given in terms of the hyperfine matrix *A*, which describes the coupling of the electron with the nuclear spin.

RESULTS AND DISCUSSION

EPR spectra of N centres in doped tin oxide. The as-prepared N-SnO_2 material shows a weak EPR spectrum whose intensity, however, grows upon a further thermal treatment directly performed in the EPR cell. This consists in an annealing under vacuum at 773 K followed by a treatment in 100 mBar pure oxygen for 1 hour at the same temperature. This treatment allows to recover the optimal oxidation state of the material. Indeed, it tends to spontaneously lose very small amounts of oxygen leaving excess electrons in the solid, which are scavenged by low-laying trapping states by N paramagnetic centres, which become therefore diamagnetic by addition of an electron (see below). This behaviour corresponds exactly to a similar process experienced in the case of nitrogen doped TiO_2.[30]

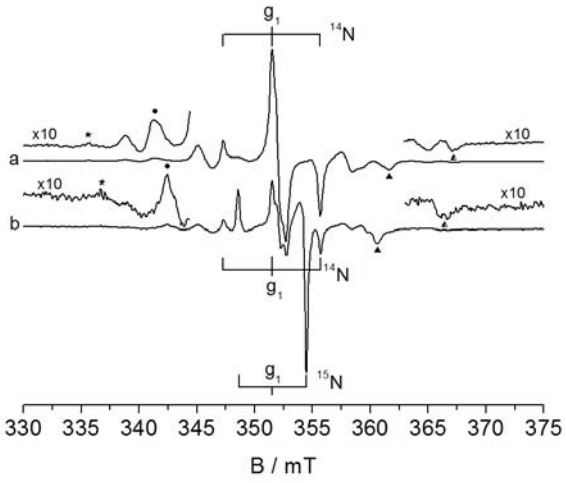

Figure 1: EPR spectra recorded at 77K of the N center in SnO_2. a) X-band spectrum of a sample containing ^{14}N; b) X-band spectrum of a sample containing 70% of ^{15}N. The stick diagrams indicate the nitrogen hyperfine coupling corresponding to the g_1 component. The symbols ★●▲◭ highlight the other EPR features affected by the isotopic exchange.

The EPR spectrum recorded after the aforementioned thermal treatment (Figure 1) is due to a nitrogen based paramagnetic centre located in the bulk of the solid. No broadening of the signal is observed when the spectra are recorded at 77K under oxygen atmosphere. This allows to exclude the surface nature of the paramagnetic centre. Figure 1 compares the X-band spectra (microwave frequency, v = 9.50GHz) obtained using $^{14}NH_4Cl$ (100%) (Figure 1a) or a mixture of $^{14}NH_4Cl$ (30%) and $^{15}NH_4Cl$ (70%), Figure 1b, in the preparation of the solid. The two nitrogen isotopes have nuclear spin I = 1 (^{14}N) and I = ½ (^{15}N), respectively. Thus, in the case of centres having one single N atom, one expects EPR signals based on triplets of hyperfine lines for ^{14}N (2I + 1 = 3) or signals based on doublets of lines (^{15}N, 2I + 1 = 2). This is exactly what is shown in Figure 1, where the stick diagrams indicate the presence of a triplet ascribed to ^{14}N containing centre (Figure 1a) and of a doublet attributed to ^{15}N (Figure 1b). In this latter case, the trace of the ^{14}N triplet (30%) is still observed. The coupling constants, preliminary measured from the spectral traces, are 4.2 mT (^{14}N, 99.63% natural abundance) and 5.9 mT (^{15}N, 0.366% natural abundance). The ratio between the two coupling constants is that expected on the basis of the ratio between the nuclear *g* factors of the two isotopes. We have also recorded (*vide infra*) X-band EPR spectra for a sample containing 98% of ^{15}N and spectra in the Q-band mode (35 GHz, ^{14}N). At this frequency the various ***g*** components of a signal are more separated due to the stronger magnetic field of the experiment, while the hyperfine separations remain unaffected.

The only nitrogen component is not sufficient to explain the whole rich hyperfine structure of the spectra reported in Figure 1. Other lines appearing at the external wings of the spectrum results from the interaction of the unpaired electron with tin nuclei. The two more abundant tin isotopes having non-zero nuclear spin are ^{117}Sn (7.75% natural abundance) and ^{119}Sn (8.6% natural abundance). Both isotopes have nuclear spin I = ½ so that, even though their nuclear *g* factor is slightly different, we can, for the sake of simplicity, consider the presence of a unique magnetic tin nucleus with I = ½ and natural abundance 16.35%, hereafter indicated with *Sn. The tin hyperfine lines are not due to an independent signal. They rather belong to the same signal showing the nitrogen hyperfine lines discussed above. This can be understood considering the shift observed for these lines (some of them are evidenced in the figure) passing from Figure 1a to Figure 1b. The shift exactly corresponds to the difference in the position between the outer lines of the ^{15}N and ^{15}N hyperfine structures, respectively. We are thus in the presence of a complex EPR signal resulting from a paramagnetic centre in which the unpaired electron interacts with both N and Sn atomic species. Consequently, this suggests that the N defect is included into the oxide structure as an anionic dopant.

Leaving to the following of this paper (Section 4) the discussion about the exact nature of the doping centre, i.e. whether N takes the place of O into the lattice or it binds to oxygen forming a sort of NO^{x-} charged moiety (example of both types of centres have been observed in N doped oxides),[31,32] we can now consider the simulation of the experimental EPR spectrum temporarily assuming an N atom in the crystallographic position of oxygen in the tin oxide lattice (Scheme 1a). Since SnO_2 has the rutile structure, each anion is surrounded by three Sn^{4+} cations.

Scheme 1

a) b)

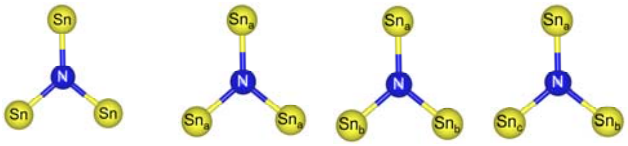

The expected EPR spectrum, in particular the *Sn hyperfine structure, is given in principle by two main factors. The first one is the structural (and magnetic) equivalence or non-equivalence of the Sn ions, in other words the symmetry of the centre. The second factor is the distribution of the magnetic *Sn nuclei around N. There are, in principle, four distinct isotopomers with zero, one, two and three *Sn ions surrounding the N centre, respectively. The number of possible cases is thus relatively high. A discussion about the expected spectral structure in all these cases must be preliminary to the simulation itself (see previous section).

Symmetry of the defective site and isotopomers distribution. As mentioned above, three models are possible to describe the symmetry of the sites: (i) all Sn ions are structurally and magnetically equivalent, (ii) two of them only are equivalent while the third is not and, (iii) all Sn ions are non-equivalent.

The three cases are represented in Scheme 1b. We will use in the following the simplified notations: (i) $NSn_aSn_aSn_a$; (ii) $NSn_aSn_bSn_b$; (iii) $NSn_aSn_bSn_c$.

In general terms, the probability of finding m magnetic isotopes of tin (*Sn, I = ½, abundance p = 0.1635) in an array of n Sn atoms is given by

$$P_n(m) = \binom{n}{m} p^{n-m} q^m$$

with $p = 1 - q$. In our case p = 0.1635, q = 0.8365, (m= 1,2,3), n= 3. The $\binom{n}{m}$ term is:

$$\binom{n}{m} = \frac{n!}{m!\,(n-m)!}$$

The distributions of the four more abundant isotopomers for the three possible models of the site are resumed in Table 1.

It comes obvious from the Table 1(column 3-5) that the abundance of the various isotopomers containing magnetic tin nuclei, which is one of the factors determining the intensity of the corresponding hyperfine structure, is different in the three cases.

Table 1: The four main isotopomers for each of the three possible structural models of the N centre are reported with their expected abundance. The magnetic (I ≠ 0) nuclei are in bold.

Model	Isotopomer/ abundance			
1- N Sn_a Sn_aSn_a	**N** $Sn_aSn_aSn_a$/ 0.582	**N** ***Sn_a**Sn_aSn_a/ 0.345	N ***Sn_a**-***Sn_a**Sn_a/ 0.068	N ***Sn_a**-***Sn_a**-***Sn_a**/ 0.0045
2- N Sn_a Sn_bSn_b	**N** $Sn_aSn_bSn_b$/ 0.582	**N** Sn_a-***Sn_b** Sn_b/ 0.23	**N** ***Sn_a**Sn_bSn_b/ 0.115	N ***Sn_a**-***Sn_b**Sn_b/ 0.045
3- N Sn_a Sn_b Sn_c	**N** $Sn_aSn_bSn_c$/ 0.582	**N** ***Sn_a**Sn_bSn_c / 0.115	**N** Sn_a-***Sn_b** Sn_c / 0.115	**N** Sn_aSn_b-***Sn_c**/ 0.115

Since the experimental spectrum results from the overlap of the signals of all isotopomeric species present in the system, the computer simulation has been conducted optimizing, first, the spectra of the species non containing *Sn nuclei (Figure 2a and second column in Table 1). This species (**N**SnSnSn) is the most abundant in all cases and its hyperfine structure is due uniquely to nitrogen. The first step of the simulation allows, thus, to describe the main species as characterized by a rhombic symmetry with a weakly anisotropic ***g*** tensor (g_1 = 2.0053, g_2 = 2.0023, g_3 = 1.9978) and a hyperfine ***A*** tensor due to ^{14}N with a relevant coupling in one direction only and very small couplings in the other two directions (A_1 = 4.17 mT, A_2 = 0.08 mT, A_3 = 0.08 mT). This is the typical situation of radical centres containing the unpaired electron in a *p* orbital of t N atom.

In a second step, we have introduced magnetic tin nuclei in the simulation, starting from reproducing the isotopomer with one magnetic tin *Sn, third column of Table 1, which is the second centre in terms of abundance among the three models reported in Table 1. Both magnetic isotopes (^{117}Sn, ^{119}Sn) have I = ½ and the corresponding hpcc are usually high due to the very large value of the corresponding atomic constants of tin. Since the N coupling constants A_2 and A_3 are very small in comparison to the linewidth of the signal, one expects for these components a simple splitting in two lines caused by tin. By contrast, in the case of the component in the direction of g_1 (A_1), one expects a splitting in two lines for each of the N hyperfine lines. The hyperfine structure of this second isotopomer, containing one *Sn atom (**N*Sn_a**Sn_aSn_a), is thus in theory composed by ten lines. We have achieved a satisfactory simulation (Figure 2b) of most of the missing lines introducing, in this second step, *Sn coupling constants higher than 11 mT in all directions (Table 2) and considering an abundance of this isotopomer of about 60% of the first one. This corresponds to the value expected for model 1 in Table 1.

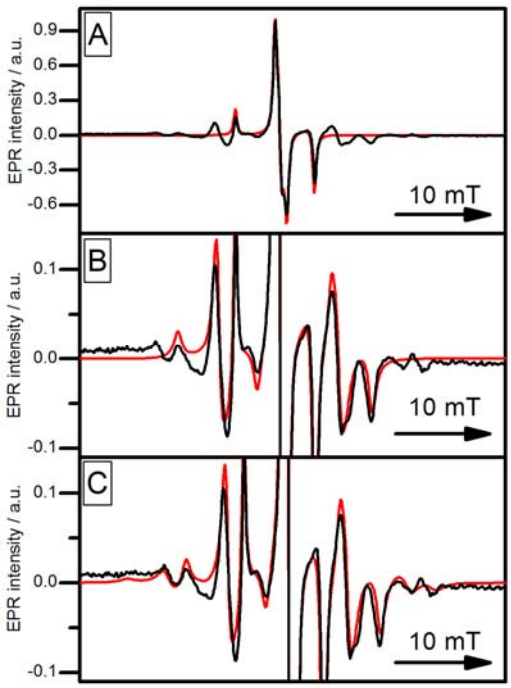

Figure 2: EPR spectra recorded at 77K and the simulated trace (in red) of the N center in SnO_2. a) X-band spectrum simulated considering the ^{14}N coupling only; b) magnification of the X-band spectrum simulated considering also the isotopomer with one *Sn nucleus (**N*Sn$_a$**Sn$_a$Sn$_a$). c) Magnification of the X-band spectrum simulated considering also a second isotopomer with two equivalent *Sn nuclei (**N*Sn$_a$*Sn$_a$**Sn$_a$).

The simulation was then refined by introducing a third component having two magnetic tin nuclei with the same hyperfine constants used in the previous step (**N*Sn$_a$*Sn$_a$*Sn$_a$**) and with a low abundance (about 7% of the total paramagnetic centres). The external weak lines of the spectrum, not reproduced by the previous simulations (Figs 2A and 2B) are in this way accounted for (magnification in Figure 2C). The last isotopomer (three magnetic *Sn, Table 1, column 5) has negligible abundance and has not been considered.

Figure 3 provides an overall view of all the simulations by comparing the experimental and the simulated traces for ^{14}N (X-band, Figure 3a), ^{15}N (X-band, Figure 3b) and ^{14}N (Q-band, Figure 3c). In all cases the same set of parameters (**g** and **A**) was used. The agreement between the experimental and simulated spectra is more than satisfactory.

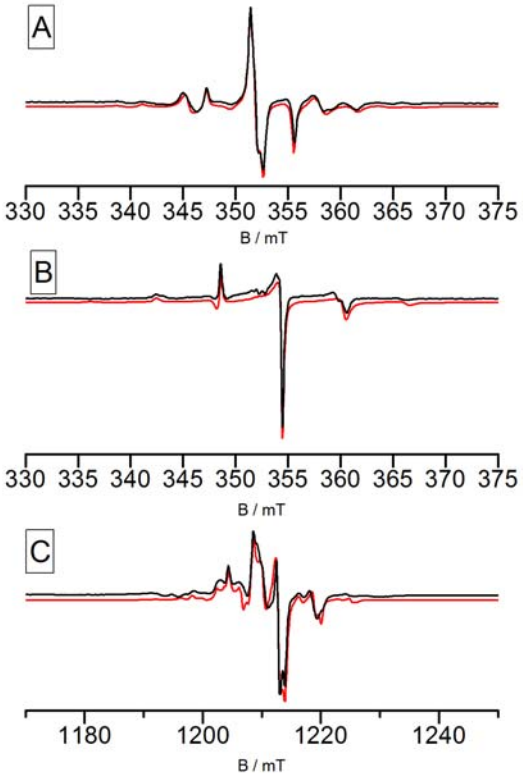

Figure 3: EPR spectra recorded at 77K and simulations of the N centre in SnO_2. X-band spectrum of a sample containing ^{14}N (A), X-band spectrum of a sample containing ^{15}N (98%) (B) and Q-band spectrum of the sample in A (C).

Table 2: Spin Hamiltonian parameters (mT) for the N-SnO_2 paramagnetic centre.

g_1	g_2	g_3	Nucleus	A_1	A_2	A_3
2.0053	2.0023	1.9978	^{14}N	4.17	0.083	0.078
			^{15}N	5.88	0.117	0.110
			^{119}Sn	12.2	12.8	12.4
			^{117}Sn	11.7	12.3	11.9

Indeed, the results of the spectra analysis indicate that, among the three possible models discussed above, the first one, having three equivalent tin ions around the nitrogen centre (NSn$_a$Sn$_a$Sn$_a$), is the structural model corroborating exactly the experimental spectra. The factors that clearly support our interpretation are: i) the correct position of the weak Sn hyperfine lines and ii) the correct intensity ratio between the hyperfine lines of three isotopomers with zero, one, and two magnetic tin nuclei, respectively. This is not the case for the two other models.

To summarize, the complex simulation of the EPR spectra of the N centre in SnO_2 highlights a rather symmetric structure including three equivalent tin ions surrounding nitrogen (model 1 in Table 1). For the sake of clarity, however, we must note that a similar spectral structure could be obtained using model 3 (N Sn$_a$ Sn$_b$

Sn_c) provided that the hyperfine constants of the three inequivalent tin ions are very closed one to the other. In such a case, the three independent isotopomers reported in Table 1, columns 3-5, having one magnetic tin nucleus and an abundance of 0.115 each, would merge into an unresolved structure having an abundance of 0.345, which is exactly the case for the model 1. We can thus also conclude that the three tin ions surrounding N are magnetically equivalent. Alternatively, the three ions could be slightly inequivalent with a degree of magnetic non equivalence which is so small to be undetectable from the EPR powder spectra.

Spin density of the N center in SnO_2. The spin density on the nitrogen atom of the N centre in SnO_2 can be derived from the hyperfine matrix **A** (Table 2) according to:

$$A = \begin{vmatrix} A_1 & 0 & 0 \\ 0 & A_2 & 0 \\ 0 & 0 & A_3 \end{vmatrix} = a_{iso} + \begin{vmatrix} 2T & 0 & 0 \\ 0 & -T & 0 \\ 0 & 0 & -T \end{vmatrix}$$

$$= 1.44 + \begin{vmatrix} 2.73 & 0 & 0 \\ 0 & -1.36 & 0 \\ 0 & 0 & -1.36 \end{vmatrix}$$

where a_{iso} is the Fermi contact term (proportional to the electron spin density in the nuclear volume) and ***T*** is the dipolar matrix having the typical form of the electron-nucleus dipolar interaction for an electron in a p orbital (i.e., *2T*, *-T*, *-T*). The spin density in the *p* orbital, calculated by comparison of the experimental values with the corresponding atomic value (ρ(2p)= *T*/*T*°) is thus mainly localized (0.687) on a N 2*p* orbital (*T*° = 1.981 mT). The isotropic Fermi contact term is expected to be positive in N-centred radical species and indicates a further amount of electron spin density (0.022) in the 2*s* orbital of the nitrogen atom. The total spin density on the N atom of the observed species amounts therefore to 0.71, with the larger contribution being due to a single 2*p* orbital.

An analogous calculation for the spin density on Sn shows that the interaction is dominated by the a_{iso} term (11.9 mT in the case of the ^{117}Sn isotope). Despite this relatively large value, the comparison with the huge atomic constant of tin (1498 mT) indicates a weak effect in terms of spin density on the 5*s* orbital of Sn which totals to about 0.008. The analysis of the dipolar component is less reliable owing to the strong error affecting the T matrix term, which becomes very small after extraction of the a_{iso} component. In any case, the experimental T value should be in the order of 0.1-0.2 mT, again indicating a weak "trough space" dipolar interaction between the electron, mainly confined on the N atom, and the surrounding Sn ions. This aspect of the interaction will be better discussed in the following based on first principles DFT calculations.

DFT calculations of N centres in doped tin oxide.

Calibration of Sn all electron basis set. To limit the calculation to valence electrons, effective core potentials (ECPs) are usually adopted. However, in case of inner shell properties, such as hyperfine coupling constants, all electron basis sets are needed. This is the case of the hyperfine interactions at Sn atoms, which thus requires an appropriate description of the atomic core shell.

Unfortunately, all electron basis sets for Sn for periodic systems are not available in the literature. An accurate qualitative assessment of newly developed all electron basis sets with respect to properties like the hyperfine constants is mandatory. To this purpose, EPR data for three different Sn molecular radicals were considered as a benchmark, since accurate experimental data exist.[33] Here, a(Sn) denotes the average value of A_1, A_2 and A_3, because only well-resolved isotropic spectra could be obtained experimentally. The A tensor was computed by employing four molecular and six periodic adapted all electron basis sets with increasing accuracy, from 3-21G to valence quadruple zeta plus polarization (QZP, for more details see Supplementary Information). Starting from molecular all electron basis sets, we constructed a new well balanced basis set for solid systems.

The three considered radicals belong to three distinct groups having different a(Sn) values: (i) a $R_3Sn^{\bullet}$ radical type with a(Sn) ≥ 190 mT, which is mostly direct contact interaction; (ii) $R_3SnC^{\bullet}R_2$ with a(Sn) 13-16 mT, attributed to spin polarization through Sn—C bond, and (iii) $R_3SnCH_2C^{\bullet}H_2$, which shows a(Sn) 42-47 mT, probably deriving from some hyperconjugation, although direct overlap of the odd-electron orbital with tin orbitals is also possible. In this way, we are able to evaluate the basis set accuracy in all the possible cases. As discussed in detail in the next Section, the analysis of the structure and the spin distribution in N-doped SnO_2, indicate that this system is analogous to the species in group (ii), i.e. those where the paramagnetic center is nearest neighbour to the Sn atom. Therefore, the unpaired electron gives rise to a super-hyperfine interaction with the Sn atom being localized on a neighbouring N atom. For the sake of brevity, in Table 3, the results obtained with only two BS are reported: a valence double-ζ (DZV) and a valence quadruple-ζ plus polarization (QZP) basis set, both adapted for periodic systems. Additional data are available in the Supporting Information.

Table 3: Experimental[33] and calculated ^{117}Sn Fermi contact interaction, a(^{117}Sn) (mT), of three tin radicals and module of the percentage difference with respect to the experiment value.

	a (^{117}Sn), mT				
	Expt[(a)]	DZV	Δ%	QZP	Δ%
$(CH_3)_3Sn^{\bullet}$	189.9	-411.43	116.7	-184.07	3.1
$(CH_3)_3SnC^{\bullet}H_2$	13.25	10.64	19.7	10.78	18.6
$(CH_3)_3SnCH_2C^{\bullet}H_2$	46.77	-35.19	24.8	-41.06	12.2

(a) The sign cannot be determined experimentally

It is noteworthy that only the a(Sn) value of the radical, for which the electron spin density is directly localized on the tin atom, i.e. $(CH_3)_3Sn^{\bullet}$, strongly depends on the size of the basis set. The other two radicals have the unpaired electron on a first or second neighbour C atom, respectively, and the a(Sn) value is of course much less affected. However, the quality of the basis set is essential for a proper reproduction of a(Sn) as expected. In particular, the DZ basis set is clearly insufficient, especially for $(CH_3)_3Sn^{\bullet}$, with an error of 117% (Table 3). The more flexible QZP basis set, on the contrary, provides an almost quantitative agreement with the experiment in all

the three cases (3% error, Table 3). Based on these results, the latter BS will be used for the calculation of Sn hyperfine constants in N-SnO_2.

Structural Model and Electronic Properties. In this section, we report three possible models (Figure 4) of N-doped SnO_2. In particular, we considered one substitutional (N_{sub}) and two interstitial ($N_{int}1$ and $N_{int}2$) structures of N impurities in the SnO_2 rutile bulk structure. Substitutional N-doping was modelled by replacing one single O atom in the supercell, while the interstitial ones are obtained by adding one N atom in the supercell. According to other oxide systems,[12] the substitution of a lattice oxygen with a nitrogen atom does not lead to remarkable changes in the structure. On the contrary, the insertion of an interstitial N involves the formation of NO species with three electrons localized in the π antibonding orbitals.[13] The structural reorganization due to the N inclusion is slightly different in the two cases. In $N_{int}1$ (Figure 4c), N is bound to one O and two Sn atoms; in $N_{int}2$ N is bound to one O and to one Sn atom (Figure 4d). The two models differ in energy, the first one being more stable by 0.8 eV per supercell. The N—O bond length is of 1.34 Å and 1.43 Å, respectively, very close to N-TiO_2 results.[13,31]

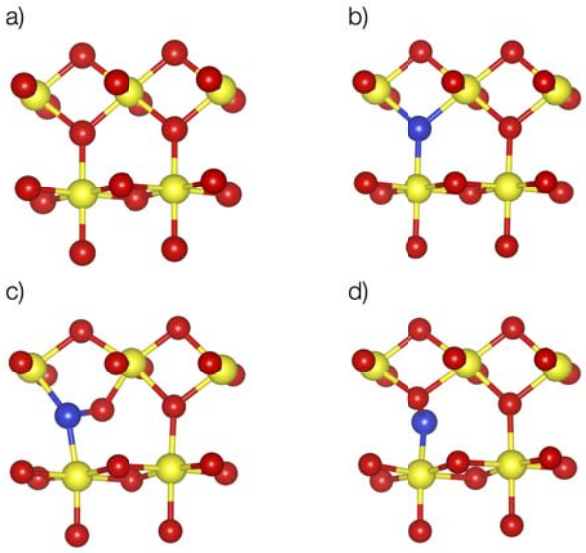

Figure 4: Structural model of undoped SnO_2 (a), substitutional (b) and interstitial (c, d) N-doped SnO_2 models. Blue represents N atoms, yellow Sn and red O.

The density of states (DOS) of N_{sub} and $N_{int}1$ defect structures are reported in Figure 5. N_{sub} introduces a singly occupied N $2p_\alpha$ state, which lies below the top of the O 2*p* valence band (VB), in agreement with previous studies.[7,8] This state is not localized on N atom, but we can observe a hybridization between N 2*p* and O 2*p* band states. The corresponding empty $2p_\beta$ component (hole state), instead, is fully localized on the N 2*p* state and lies just below the bottom of the CB (Figure 5a). However, not much emphasis has to be given to Kohn-Sham one-electron eigenfunctions, as they are constructed for a noninteracting reference system. These, indeed, have no physical meaning, contrary to exact many-body wavefunction. The total and spin density (computed as difference between alpha density and beta density) instead is the same as that of the interacting electrons and then can be reasonably discussed (see below).

$N_{int}1$ is associated to a singly occupied π MO which lies 0.76 eV above the top of the VB (Fig. 5 top). The corresponding empty component is also very high in the band gap and merges with the CB, Figure 5. The large energy separation between the filled and empty components of the impurity state indicates a strong exchange splitting which is typical of highly localized unpaired electrons.

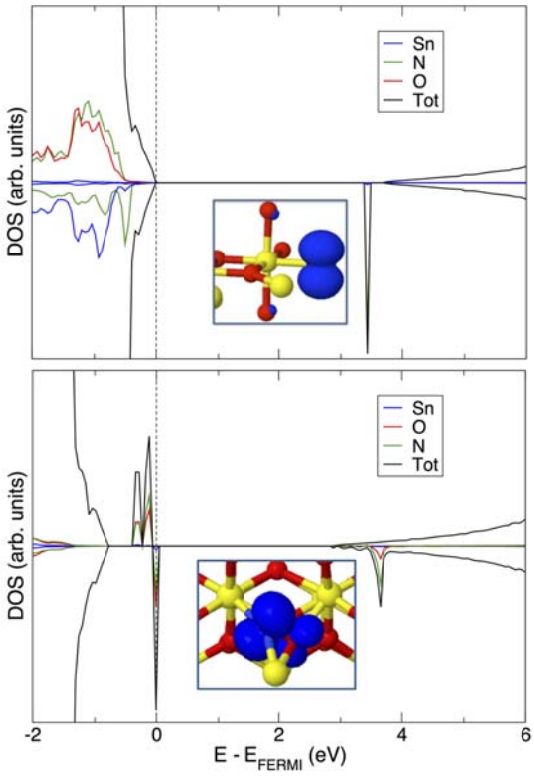

Figure 5: DOS curves of N_{sub} (top) and $N_{int}1$ (bottom) dopants in N-SnO_2. Spin density plots (isodensity threshold values 0.005) are reported as inserts.

In Table 4, ^{14}N and ^{117}Sn hpcc for the three doped systems shown in Figure 4 are reported (^{15}N and ^{119}Sn data are available in SI). The agreement between the computed and measured ^{14}N values (see tensor **A** in Table 4) is quite satisfactory for both the N substitutional and N interstitial arrangements. In the N_{sub}–SnO_2 structure, the spin density is completely localized (0.99 e) on the N atom (Figure 5), more precisely on the *p* state perpendicular to the plane defined by the three Sn atoms bound to N. Otherwise, in the N_{int} systems, the unpaired electron is shared between the N and O atoms of the NO species (Figure 5); the spin density is localized on the π system, thus reducing the localization to 0.67 and 0.89 for $N_{int}1$ and $N_{int}2$, respectively, as already observed in the parent N-TiO_2 system.[13,31] Despite the different values of ρ in the three systems, the ^{14}N hpcc are quite similar.

It is clear that the calculations tend to overestimate the a_{iso} term, while they accurately reproduce the **T** tensor. These values are similar for all the doped systems. However, $N_{int}1$ and $N_{int}2$ show a slight asymmetry between T_2 and T_3, which is not observable in the experimental data. As in the N-TiO_2 case, the simple comparison of the computed and measured N hyperfine constants is not sufficient to conclude on the nature of the doping element, either substitutional or interstitial, owing to the similarity of the values.

Table 4: Experimental and calculated ^{14}N hyperfine coupling constants (mT) and spin density (ρ).

	A_1	A_2	A_3	a_{iso}	T_1	T_2	T_3	ρ
N_{sub}	4.588	0.439	0.420	1.820	2.772	-1.377	-1.395	0.99
$N_{int}1$	4.068	0.445	0.365	1.626	2.442	-1.181	-1.261	0.76
$N_{int}2$	4.597	0.355	0.230	1.728	2.870	-1.373	-1.497	0.89
Expt (Table 2)	4.170	0.083	0.078	1.44	2.726	-1.360	-1.366	0.71

In order to shed the light on the nature of the N dopant, one can further consider the computed ^{117}Sn (super)hyperfine coupling constants. Note that the corresponding ^{119}Sn constants are reported in SI. For each model, N_{sub}, $N_{int}1$, and $N_{int}2$, the values for the three Sn atoms nearest neighbours to N are reported in Table 5 and Figure 6. In the N-substitutional structure, the three Sn atoms are all bound to N with similar distances and show similar **A** values. In particular, Sn1—N, with bond length of 2.113 Å, has **A** tensor values slightly lower than Sn2 and Sn3 (Table 5). On the contrary, in the N-interstitial systems, we find two non-equivalent Sn species around the N dopant: 1) Sn directly bound to N (i.e Sn1), with coupling constants similar to Sn in the N_{sub} system, and 2) Sn bound to O atom, which shows negative a_{iso} (Sn2 and Sn3). In this latter case, hyperconjugation is present and positive spin density, is computed, as in the $(CH_3)_3SnCH_2C^{\bullet}H_2$ radical (group (iii) see above).

Table 5: Experimental and calculated ^{117}Sn superhyperfine coupling constants (mT) and spin density (ρ).

	Sn	A_1	A_2	A_3	a_{iso}	T_1	T_2	T_3	ρ
	1	8.235	9.192	8.391	8.606	-0.371	0.585	-0.225	-0.018
N_{sub}-SnO_2	2	8.785	9.764	8.799	9.116	-0.331	0.648	-0.317	-0.024
	3	8.781	9.759	8.794	9.111	-0.330	0.648	-0.317	-0.024
	1	7.555	8.355	7.685	7.865	-0.310	0.490	-0.180	-0.015
$N_{int}1$-SnO_2	2	2.866	3.821	3.421	3.369	-0.503	0.451	0.052	-0.009
	3	-11.437	-9.578	-9.636	-10.217	-1.220	0.639	0.581	0.008
	1	15.096	16.147	15.192	15.478	-0.382	0.669	-0.286	-0.017
$N_{int}2$-SnO_2	2	-2.192	-1.562	-1.770	-1.842	-0.351	0.280	0.071	0.003
	3	-2.456	-1.819	-2.013	-2.096	-0.360	0.277	0.083	0.003
Expt		11.67	12.29	11.88	11.946	-0.277	0.344	-0.067	

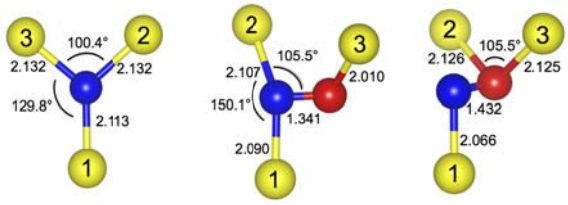

Figure 6: Local structural features of three N-doped SnO_2 structures: N_{sub}, $N_{int}1$ and $N_{int}2$. Bond length (Å) and angles (degree) are reported. Labels refer to Table 5.

DISCUSSION AND CONCLUSIONS

In this study we have reported for the first time an accurate characterization of the paramagnetic centres formed in SnO_2 when this semiconducting oxide is doped with nitrogen. The samples obtained by precipitation followed by thermal annealing treatment exhibit a very complex EPR spectrum, which is characteristic of the N-doped material. The EPR signal stems clearly from paramagnetic species in which the unpaired electron interacts with both N and Sn atoms, suggesting

that the N defect is included in the oxide structure as an anionic dopant. This could be either a N atom replacing a lattice oxygen (substitutional nitrogen) or a N atom in an interstitial position (interstitial nitrogen).

The complex simulation of the EPR spectra of N-doped SnO_2 suggests that the N dopants form a rather symmetric structure, with three equivalent Sn ions surrounding the nitrogen impurity ($NSn_aSn_aSn_a$). However, a similar spectral structure could arise assuming three non-equivalent Sn atoms around the N impurity ($NSn_aSn_bSn_c$), provided that the hyperfine constants of the three Sn ions are very similar, and cannot be resolved due to the complexity of the structure. The conclusion derived from the present analysis is that the three tin ions surrounding N are magnetically equivalent or, alternatively, have a degree of non-equivalence which is so small to be undetectable from the features of the experimental EPR powder spectra.

In order to gain further insight on the nature of the N-dopants, we have performed DFT calculations on the electronic structure of N-SnO_2 using the B3LYP hybrid functional. Substitutional nitrogen and two variants of interstitial nitrogen have been investigated by optimizing a bulk supercell containing 72 atoms. The results demonstrate that in the case of substitutional nitrogen a N 2*p* orbital is singly occupied; the unpaired electron is strongly localized on the N dopant. Interstitial nitrogen results in two slightly different N-O structures with an unpaired electron occupying a NO π orbital.

The computed hyperfine and superhyperfine constants for the substitutional case reproduce the general features of the EPR spectra with the unpaired electron interacting with two species (N and Sn). The three Sn atoms around N show a very similar **A** tensor and are not exactly equivalent, but their properties are very close with two Sn atoms exhibiting virtually identical **A** tensors, and one slightly different Sn atom. This suggests that the computed model of a substitutional nitrogen shows two long and one short N—Sn distances.

The **A** tensor computed for the N_{int} centres is characterized by strong anisotropy which reflects the geometrical structure around the N dopant. The three Sn atoms display significantly different hyperfine interactions in contrast to the experimental observation. Therefore, considerations based on simple symmetry and equivalence arguments clearly point towards the formation of an N substitutional dopant.

Further support to this conclusion comes from a quantitative analysis of the measured and computed hyperfine constants. The ^{14}N hpcc shows that N_{sub}, $N_{int}1$, and $N_{int}2$ species possess similar **A** tensors, Table 4. The experimental values are reproduced with high accuracy, confirming the high localization of the unpaired electron on the N dopant or on the N—O complex. However, whereas the correspondence between computed and measured values is slightly better for the N_{sub} case, the differences are too small to provide a conclusive assignment as far as the position of the dopant, substitutional or interstitial, is concerned.

Much more relevant is the analysis of the Sn hyperfine coupling constants. Here the calculation of these quantities from first principles becomes more complicated by the large core of the Sn atom and by the necessity to use a sufficiently flexible basis set to describe the core levels. Furthermore, the use of an all electron basis set, required to compute the EPR properties, results in the neglect of scalar relativistic effects. Nevertheless, a careful comparison with a set of Sn-containing paramagnetic molecules has shown that our computed superhyperfine interactions on Sn, and in particular the dominant a_{iso} term, are underestimated by about 20%. The **A** tensor values computed for the N_{sub} centres are indeed underestimated with respect to the experimental ones (Table 5). However, if we consider the $\approx$20% correction obtained from the study on the Sn radicals, we obtain values, which are in almost quantitative agreement with the experiments.

In conclusion, both the analysis of the complex EPR spectra and the comparison of computed (DFT) and measured hyperfine coupling constants indicate that nitrogen dopants in SnO_2 are present as substitutional to oxygen species, which are surrounded by three nearly equivalent Sn atoms. These defects introduce singly occupied states just below the top of the valence band, while the corresponding empty component lies high in the gap, close to the bottom of the conduction band. In all cases, the hole is strongly localized, a result that contrasts with the possibility to use N-SnO_2 as a d^0 ferromagnet and also is expected to result in high electron-hole recombination rates when the material is used as photocatalyst under UV-vis light. Experimental verification of the performance of the N-SnO_2 samples as active photocatalysts is planned and will be the subject of future investigations.

ASSOCIATED CONTENT

Table S1 with optimized cell parameters and band gap of all the doped and undoped structures; Table S2 reports ^{117}Sn a_{iso} computed with all the molecular and periodic adapted all electron basis sets; Table S3 gathered all the experimental and calculated ^{119}Sn superhyperfine coupling constants. “This material is available free of charge via the Internet at http://pubs.acs.org.”

AUTHOR INFORMATION

Corresponding Author

*Email: cristiana.divalentin@unimib.it

ACKNOWLEDGMENT

This work has been supported by the CARIPLO Fondation through the grant n° 2013-0615 "Novel heterojunction based photocatalytic materials for solar energy conversion" and by the Italian MIUR through the FIRB Project RBAP115AYN “Oxides at the nanoscale: multifunctionality and applications”. The support of the COST Action CM1104 “Reducible oxide chemistry, structure and functions” is also gratefully acknowledged.

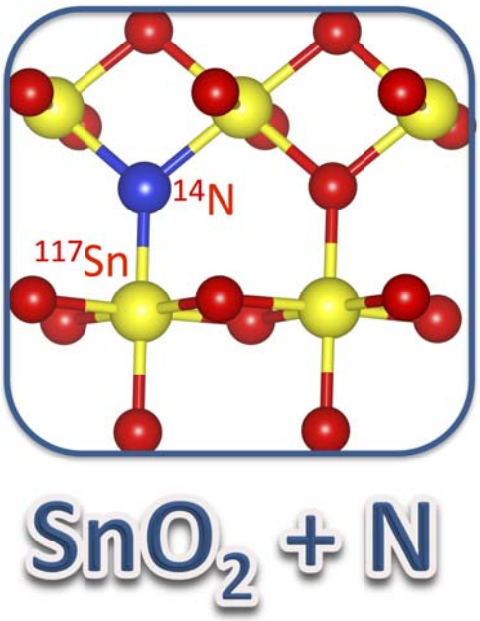
^{14}N
^{117}Sn
SnO_2 + N

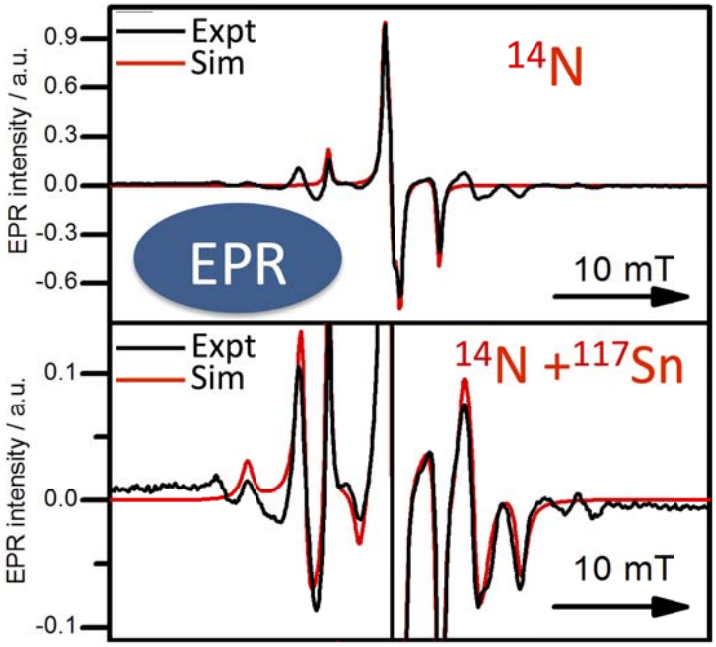
Expt
Sim
^{14}N
EPR
10 mT
EPR intensity / a.u.
0.9
0.6
0.3
0.0
-0.3
-0.6
Expt
Sim
^{14}N +^{117}Sn
10 mT
EPR intensity / a.u.
0.1
0.0
-0.1

REFERENCES

[1] Batzill, M.; Diebold, U. The surface and materials science of tin oxide. *Prog. Surf. Sci.* **2005**, *79*, 47-154.

[2] Idota, Y.; Kubota, T.; Matsufuji, A.; Maekawa, Y.; Miyasaka, T. Tin-Based Amorphous Oxide: A High-Capacity Lithium-Ion-Storage Material. *Science* **1997**, *276*, 1395-1397.

[3] Gubbala, S.; Chakrapani, V.; Kumar, V.; Sunkara, M. K. Band-Edge Engineered Hybrid Structures for Dye-Sensitized Solar Cells Based on SnO_2 Nanowires. *Adv. Funct. Mater.* **2008**, *18*, 2411-2418.

[4] Kowal, A.; Li, M.; Shao, M.; Sasaki, K.; Vukmirovic, M. B.; Zhang, J.; Marinkovic, N. S.; Liu, P.; Frenkel, A. I.; Adzic, R. R. Ternary Pt/Rh/SnO_2 electrocatalysts for oxidizing ethanol to CO_2. *Nature Mater.* **2009**, *8*, 325-330.

[5] Pan, S. S.; Ye, C.; Teng, X. M.; Li, L.; Li, G. H. Localized exciton luminescence in nitrogen-incorporated SnO_2 thin films. *Appl. Phys. Lett.* **2006**, *89*, 051911.

[6] Pan, S. S.; Wang, S.; Zhang, Y.X.; Luo, Y. Y.; Kong, F. Y.; Xu, S. C.; Xu J. M.; Li, G.H. p-type conduction in nitrogen-doped SnO_2 films grown by thermal processing of tin nitride films. *Appl Phys A* **2012**, *109*, 267–271.

[7] Long, R.; English, N. J. Density functional theory description of the mechanism of ferromagnetism in nitrogen-doped SnO_2. *Physics Letters A* **2009**, *374*, 319–322.

[8] Xiao, W. Z.; Wang, L. L.; Xu, L.; Wan, Q.; Zou, B. S. Magnetic properties in Nitrogen-doped SnO_2 from first-principle study. *Solid State Communications* **2009**, *149*, 1304-1307.

[9] Wang, H; Rogach, A. L. Hierarchical SnO_2 Nanostructures: Recent Advances in Design, Synthesis, and Applications. *Chem. Mater.* **2014**, *26*, 123–133.

[10] Tricoli, A.; Graf, M; Pratsinis, S. E. Optimal Doping for Enhanced SnO_2 Sensitivity and Thermal Stability. *Adv. Funct. Mater.* **2008**, *18*, 1969–1976.

[11] Zhang, S.; Li, J.; Niu, H.; Xu, W.; Xu, J.; Hu, W.; Wang, X. Visible-Light Photocatalytic Degradation of Methylene Blue Using SnO_2/α-Fe_2O_3 Hierarchical Nanoheterostructures. *ChemPlusChem* **2013,** *78***,** 192–199.

[12] Di Valentin C.; Pacchioni, G. Spectroscopic Properties of Doped and Defective Semiconducting Oxide from Hybrid Density Functional Calculations. *Acc. Chem. Res* **2014**, *47*, 3233-3241.

[13] Di Valentin, C.; Finazzi, E.; Pacchioni, G.; Selloni, A.; Livraghi, S.; Paganini, M. C.; Giamello, E. N-doped TiO_2: theory and experiment. *Chemical Physics* **2007**, *339*, 44-56.

[14] Wen, Z.; Wang, G.; Lu, W.; Wang, Q.; Zhang, Q.; Li, J. Enhanced Photocatalytic Properties of Mesoporous SnO_2 Induced by Low Concentration ZnO Doping. *Crystal Growth & Design* **2007**, *7*, 1722–1725.

[15] Jia, T.; Wang, W.; Long, F.; Fu, Z.; Wang, H.; Zhang, Q. Synthesis, Characterization, and Photocatalytic Activity of Zn-Doped SnO_2 Hierarchical Architectures Assembled by Nanocones. *J. Phys. Chem. C* **2009**, *113*, 9071–9077

[16] Pan, S. S.; Ye, C.; Teng, X. M.; Fan, H. T.; Li, G. H. Preparation and characterization of nitrogen-incorporated SnO_2 films. *Appl. Phys. A: Mater. Sci. Process* **2006**, *85*, 21-24.

[17] Pan, S. S.; Zhang, Y.X.; Teng, X. M.; Li, G. H.; Li, L. Optical properties of nitrogen-doped SnO_2 films: Effect of the electronegativity on refractive index and band gap. *J. Appl. Phys.* **2008**, *103*, 093103.

[18] Lopez-Luke, T.; Wolcott, A.; Xu, L. P.; Chen, S.; Wen, Z.; Li, J.; DeLaRosa, E.; Zhang, J. Z. Nitrogen-Doped and CdSe Quantum-Dot-Sensitized Nanocrystalline TiO_2 Films for Solar Energy Conversion Applications. *J. Phys. Chem. C* **2008**, *112,* 1282-1292.

[19] Pan, S. S.; Shen, Y. D.; Teng, X. M.; Zhang, Y. X.; Li, L.; Chu, Z. Q.; Zhang, J. P.; Li, G. H.; Hu, X. Substitutional nitrogen-doped tin oxide single crystalline submicrorod arrays: Vertical growth, band gap tuning and visible light-driven photocatalysis. *Materials Research Bulletin* **2009**, *44*, 2092–2098.

[20] Sun, X.; Long, R.; Cheng, X.; Zhao, X.; Dai Y.; Huang, B. Structural, Electronic, and Optical Properties of N-doped SnO_2. *J. Phys. Chem. C* **2008**, *112,* 9861-9864.

[21] Pacchioni, G. First principles calculations on oxide-based heterogeneous catalysts and photocatalysts: problems and avances. *Catalysis Letters* **2015**, *145*, 80-94.

[22] Pacchioni, G.; Frigoli, F.; Ricci, D.; Weil, J. A. Theoretical description of hole localization in a quartz Al center: The importance of exact electron exchange. *Phys. Rev. B* **2001**, *63*, 054102.

[23] Pan, S. S.; Li, G. H.; Wang, L. B.; Shen, Y. D.; Wang, Y.; Mei, T.; Hu, X. Atomic nitrogen doping and p-type conduction in SnO_2. *Appl. Phys. Lett.* **2009**, *95*, 222112.

[24] Becke, A. D. Density-functional thermochemistry. III. The role of exact exchange. *J. Chem. Phys.* **1993**, *98*, 5648.

[25] Lee, C.; Yang, W.; Parr, R. G. Development of the Colle-Salvetti correlation-energy formula into a functional of the electron density. *Phys. Rev. B* **1988**, *37*, 785.

[26] Dovesi, R.; Saunders, V. R.; Roetti, C.; Orlando, R.; Zicovich-Wilson, C. M.; Pascale, F.; Civalleri, B.; Doll, K.; Harrison, N. M.; Bush, I. J.; D'Arco, P.; Llunell, M.; Causà, M.; Noël, Y. CRYSTAL14 User's Manual (University of Torino, Torino, **2014**).

[27] Pacchioni, G.; Frigoli, F.; Ricci, D.; Weil, J. A. Theoretical description of hole localization in a quartz Al center: The importance of exact electron exchange. *Phys. Rev. B* **2001**, *63*, 054102.

[28] Durand, P.; Barthelat, J. C. A theoretical method to determine atomic pseudopotentials for electronic structure calculations of molecules and solids. *Theor. Chim. Acta* **1975**, *38*, 283-302.

[29] Causa, M.; Dovesi, R.; Roetti, C. Pseudopotential Hartree-Fock study of seventeen III-V and IV-IV semiconductors. *Phys. Rev. B* **1991**, *43*, 11937-11943.

[30] Di Valentin, C.; Pacchioni, G.; Selloni, A.; Livraghi, S.; Paganini, M. C.; Giamello, E. N-doped TiO_2: Theory and experiment. *Chem. Phys.* **2007**, *339*, 44-56.

[31] Di Valentin, C.; Pacchioni, G.; Selloni, A.; Livraghi, S.; Giamello, E. Characterization of paramagnetic species in N-doped TiO_2 powders by EPR spectroscopy and DFT calculations. *J. Phys. Chem B* **2005**, *109*, 11414-11419.

[32] Gallino, F.; Di Valentin, C.; Pacchioni, G.; Chiesa, M.; Giamello, E. Nitrogen impurity states in polycrystalline ZnO. A combined EPR and theoretical study. *J. Mat Chem.* **2010**, *20*, 689-697.

[33] Lloyd R. V.; Rogers, M. T. Electron spin resonance study of some silicon- , germanium- and tin-centered radicals. *J. Am. Chem. Soc.* **1973**, *95*, 2459-2464.